Mobility of Condensed Counterions in Ion-Exchange Membranes: Application of Screening Length Scaling Relationship in Highly Charged Environments

5 Environmental Science & Technology

6 Revised: October 30, 2023

7 Yuxuan Huang[†], Hanqing Fan[†], and Ngai Yin Yip^{*,†,‡}

- 8 [†] Department of Earth and Environmental Engineering, Columbia University, New
- 9 York, New York 10027-6623, United States
- [‡] Columbia Water Center, Columbia University, New York, New York 10027-6623,
- 11 United States

1

2

3

4

* Corresponding author: Email: n.y.yip@columbia.edu, Phone: +1 212 8542984

ABSTRACT

13

14

15

16

17

18

19

20

21

22

23

24

25

26

27

28

29

30

31

32

33

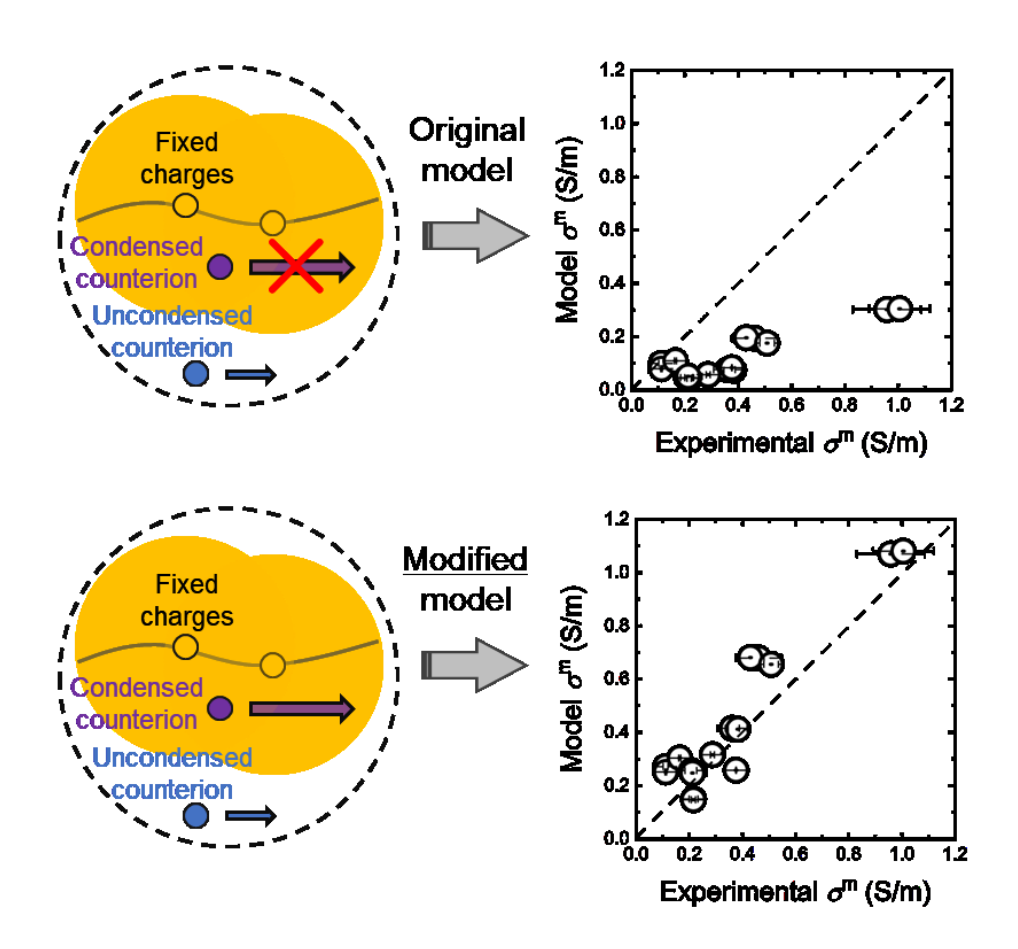
34

35

36

Ion-exchange membranes (IEMs) are widely used in water, energy, and environmental applications, but transport models to accurately simulate ion permeation are currently lacking. This study presents a theoretical framework to predict ionic conductivity of IEMs by introducing an analytical model for condensed counterion mobility to the Donnan-Manning model. Modeling of condensed counterion mobility is enabled by the novel utilization of a scaling relationship to describe screening lengths in the densely charged IEM matrices, which overcame the obstacle of traditional electrolyte chemistry theories breaking down at very high ionic strength environments. Ionic conductivities of commercial IEMs were experimentally characterized in different electrolyte solutions containing a range of mono-, di-, and trivalent counterions. Because the current Donnan-Manning model neglects the mobility of condensed counterions, it is inadequate for modeling ion transport and significantly underestimated membrane conductivities (by up to ≈5× difference between observed and modeled values). Using the new model to account for condensed counterion mobilities substantially improved the accuracy of predicting IEM conductivities in monovalent counterions (to as small as within 7% of experimental values), without any adjustable parameters. Further adjusting the power law exponent of the screen length scaling relationship vielded reasonable precision for membrane conductivities in multivalent counterions. Analysis reveals that counterions are significantly more mobile in the condensed phase than in the uncondensed phase because electrostatic interactions accelerate condensed counterions but retard uncondensed counterions. Condensed counterions still have lower mobilities than ions in bulk solutions due to impedance from spatial effects. The transport framework presented here can model ion migration a priori with adequate accuracy. The findings provide insights into the underlying phenomena governing ion transport in IEMs to facilitate the rational development of more selective membranes.

37 TOC ART



39 **KEYWORDS**

38

- 40 Ion-exchange membranes; Counterion condensation; Counterion mobility; Conductivity;
- 41 Screening length

42 **SYNOPSIS**

- 43 The novel utilization of a scaling relationship to describe screening lengths enabled the modeling
- of condensed counterion mobilities and significantly improved the accuracy of ion permeation
- 45 predictions in IEMs.

INTRODUCTION

Ion-exchange membranes, IEMs, are water-swollen polymeric films with a high density of charged functional groups.^{1–3} The membranes allow the selective transport of oppositely-charged counterions, whereas like-charged co-ions are retained through charge exclusion.^{1,2} Cation exchange membranes (CEMs) have negative fixed charges, e.g., sulfonate groups, and favor the passage of cations over anions; conversely, anion exchange membranes (AEMs) possess positive fixed charges, e.g., quaternary amines, and preferentially transport anions. The ability of IEMs to distinguish between cations and anions is utilized in numerous water, energy, and chemical production applications, including electrodialysis desalination, fuel cells, and the chloralkali process, respectively.^{4–6} Beyond the primary function of charge selectivity, i.e., between counterand co-ions, there is increasing interest in advancing IEM differentiation between counterions with different valences and between individual counterions with the same valence.^{7–9}

The charge, valence, and specific ion selectivities attainable by IEMs are determined by the transport of the different ions. Therefore, enhancing fundamental understanding of IEM transport phenomena is imperative for the rational development of more selective membranes. 9-11 Likewise, robust mechanistic transport models can be a vital tool to inform innovations in IEM selectivity. The Donnan-Manning model for IEM transport integrates the counterion condensation theory with the governing principles for Donnan potentials at solution-membrane interfaces. By modeling ion activity coefficients and mobilities in the membrane matrix, the framework can quantitatively predict ion sorption and co-ion-dominated salt permeability in IEMs. 12-14 In the model, a portion of counterions are condensed onto the fixed charges on the polymer backbone, and the condensed counterions are assumed to be immobile. 13,15,16 However, experimental observations of IEM conductivity in recent studies clearly contradict this assumption, 15,17 i.e., the evidence indicates condensed counterions are mobile. An empirical relation was put forth to relate condensed counterion mobility to ion mobility in bulk solution, but a rigorous understanding of the underlying physical meaning is lacking. 14,15 As such, there is a need for IEM transport models based on first principles that can quantitatively describe the mobility of condensed counterions.

This study develops a new model for condensed counterion mobility in IEMs and evaluates the modified transport framework against experimentally characterized ion transport. First, a theoretical model to describe condensed counterion mobility is presented, and a scaling relationship is introduced to account for screening lengths in the atypically high charge density environments within IEM matrices. Ionic conductivities of commercial cation and anion exchange membranes were characterized in a range of electrolyte solutions containing mono-, di-, and trivalent counterions. The inadequacies of the current Donnan-Manning transport framework to model membrane conductivities are discussed. We then demonstrate that incorporating the condensed counterion mobility model significantly improves the accuracy of predicted conductivities for monovalent counterions. To elucidate the influences of electrostatic interactions and spatial effect on ion permeation, counterion mobilities in condensed phase are evaluated against mobilities in uncondensed phase and bulk solution phase. Next, we put forward an explanation for the unsatisfactory mobility modeling for condensed multivalent counterions and proposed an adjustment to the screening length scaling relationship to improve model predictions for di- and trivalent counterions. Last, implications of the modified model for ion-selective separations in IEMs are discussed.

THEORY

lon Mobilities in IEMs in the Current Counterion Condensation Framework. The counterion condensation theory was originally developed to describe the colligative properties of polyelectrolyte solutions. The theoretical framework was recently extended to model ion activity and diffusion coefficients in hydrated charged polymers, i.e., IEMs, 12,13,19 and further details can be found in literature. In the model, electrostatic interactions between fixed charge groups and mobile counterions are principally governed by reduced linear charge density of the polymer, $\xi = \lambda_B/b$, where λ_B is the Bjerrum length and b is mean linear intercharge distance (Figure 1). b can be reasonably estimated from molar ratio of uncharged to charged monomers and polymer molecular architecture. When ξ exceeds the critical value of $|z_{ct}z_{fix}|^{-1}$ (z is ion valence and subscripts ct and fix denote counterion and membrane fixed charge, respectively), a fraction of the counterions, ϕ , condense onto the polymer backbone:

101
$$\phi_{c} = \frac{1 - |z_{ct}|^{-1} \xi^{-1}}{1 + v_{ct} |z_{ct}| \chi}$$
 (1)

where v is stoichiometric number of ions each electrolyte molecule dissociates into. The ratio of salt concentration in excess of fixed charge concentration relative to the fixed charge concentration in the membrane is $\chi = c_{co}^{\rm m}/v_{co}c_{\rm fix}^{\rm m}$, where c is ion concentration, subscript co indicates co-ion, and superscript m represents membrane phase. 12,14

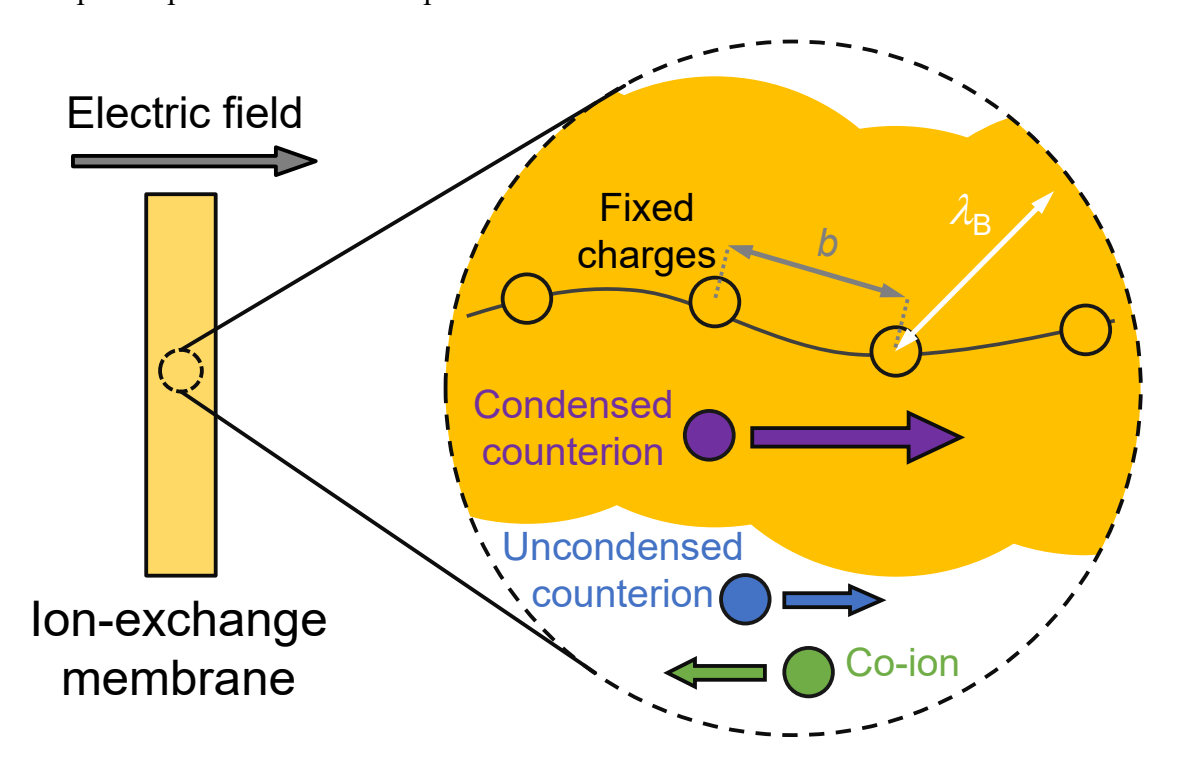


Figure 1. Schematic depicting the migration of condensed counterions, uncondensed counterions, and co-ions (violet, blue, and green circles, respectively) in IEM under applied electric field, with arrows denoting the direction of ion migration. λ_B represents the Bjerrum length, and b is the distance between fixed charges on the polyelectrolyte chains in IEM.

Correspondingly, the remaining fraction of counterions are uncondensed, $\phi_u = 1-\phi_c$. Condensed counterions are localized very close to the polymer, effectively reducing the charge density and screening the electrostatic interactions exerted by the charged moieties of the polymer matrix. Spatial effect of available fractional IEM volume for ion transport can be accounted for using the Mackie-Meares model with the factor $f_w^2/(2-f_w)^2$, where f_w is water volume fraction in the IEM. Absolute mobilities of uncondensed counterion and co-ion in the membrane, $u_{ct, u}^m$ and u_{co}^m , respectively (subscript ct, u represents uncondensed counterion), are related to the bulk mobilities, u^s (superscript s signifies bulk solution phase), using $u_{ct, u}^{13,15,21}$

119
$$u_{\text{ct, u}}^{\text{m}} = u_{\text{ct}}^{\text{s}} \left(\frac{f_{\text{w}}}{2 - f_{\text{w}}} \right)^{2} \left(1 - \frac{|z_{\text{ct}}|^{2} A}{3} \right)$$
 (2)

120
$$u_{co}^{m} = u_{co}^{s} \left(\frac{f_{w}}{2 - f_{w}} \right)^{2} \left(1 - \frac{|z_{co}|^{2} A}{3} \right)$$
 (3)

where $A \approx |z_{\rm ct}|^{-2} \Big[1 + \pi + (v_{\rm co} + v_{\rm ct}) |z_{\rm co} z_{\rm ct}| \xi \chi \Big]^{-1}$ (the approximation arose from the conversion of a summation of series to a definite integral).^{13,20} The term $1 - |z|^2 A/3$ in eqs 2 and 3 is the electrostatic effect experienced by the mobile uncondensed counterions and co-ions due to the local inhomogeneous electric field exerted by the fixed charges and condensed counterions.^{13,15,16} Note that absolute mobility can be related to diffusion coefficient, D, by multiplying u with absolute temperature and the Boltzmann constant, i.e., $D = uk_{\rm B}T$ (influence of operating temperature is accounted for).^{24,25} Further, the product of absolute mobility, valency, and the elementary charge, u|z|e, is the electrical mobility; to avoid potential ambiguity, the discussions in the study only refer to absolute ion mobility.

In the original treatment of the counterion condensation theory, condensed counterions are considered to be immobile. ^{13,15,16} However, it was noted that this assumption was unlikely to be an accurate simplification and that condensed counterions could plausibly migrate along the polyelectrolyte chain. ^{16,26,27} Condensed counterions were later categorized into "territorially" or "site" bound, with the former free to migrate in a close region along the polymer chain but unable to migrate away, whereas the latter is completely immobile. ²⁸ However, advancements in the understanding of the mobility and sub-population of the territorially bound condensed counterions are limited, ¹⁴ thus frustrating analytical quantifications of the contribution of condensed counterions to overall ionic flux. At the same time, alternative transport models have been proposed, such as one that considers condensed counterions to be immobile when the transport is driven by concentration gradients but become mobile under electric fields (the model does not differentiate between "territorially" or "site" bound). ²⁹ Rigorous justifications for such different behaviors, however, were not provided. Overall, there are presently apparent gaps in the fundamental understanding of condensed counterion mobility in IEMs that need to be addressed.

Derivation of Condensed Counterion Mobilities using a Screening Length Scaling Relationship in Concentrated Electrolytes. Previous work formulated the diffusion coefficients of condensed counterions in polyelectrolyte solutions under applied electric fields (eq S9 of the Supporting Information). Here, we further extend the theoretical framework to derive an analytical expression for the absolute mobilities of condensed counterions in IEMs, $u_{\text{ct, c}}^{\text{m}}$:

150
$$u_{\text{ct, c}}^{\text{m}} = u_{\text{ct}}^{\text{s}} \left(\frac{f_{\text{w}}}{2 - f_{\text{w}}} \right)^{2} \left[1 - 2 \left(|z_{\text{ct}}| \xi - 1 \right) \ln(\kappa b) \right]$$
 (4)

where κ is reciprocal of the screening length in the membrane matrix. 30,31 The derivation of eq 4 is detailed in the Supporting Information. Briefly, the $\left[f_{\rm w}/(2-f_{\rm w})\right]^2$ term is the Mackie-Meares parameter to account for spatial effects, 22,23 whereas the $\left[1-2(|z_{\rm ct}|\xi-1)\ln(\kappa b)\right]$ term describes the electrostatic effect on the condensed counterions by the fixed charges. Debye length, $\lambda_{\rm D}$, the characteristic distance the net electrostatic effect of a charge carrier (treated as a point source) persists for, is commonly used for $1/\kappa$ in aqueous solutions of relatively low ionic strengths. $^{31-33}$ $\lambda_{\rm D}$ scales reciprocally with square root of the ionic strength. At very high ionic strengths, $\lambda_{\rm D}$ is compressed to below the ion diameter (e.g., $>\approx$ 2.2 eq/L for Na⁺ in NaCl solution), 32,34 and the physics underpinning the Debye length breaks down (for instance, the Debye-Hückel theory for activity coefficients of ions is not appropriate for concentrated electrolyte solutions). The high charge density environments within typical IEM matrices (ionic strengths of \approx 4–11 eq/L) 37,38 are analogous to highly concentrated polyelectrolyte solutions. Employing $\kappa = 1/\lambda_{\rm D}$ in eq 4 yields unphysical negative values for $u_{\rm ct,c}^{\rm m}$. Hence, new models that are robust at high charge densities are required for the screening lengths in IEMs.

Recent studies in physical chemistry indicate that the screening length, $1/\kappa$, in concentrated electrolytes is considerably larger than the Debye length; more importantly, the studies found that $1/\kappa$ increases with solution concentration. ^{32,39,40} A scaling relationship was proposed for the screening length when the Debye length is smaller than the ion diameter, d: ^{35,36}

$$\frac{1}{\kappa \lambda_{\rm D}} = \left(\frac{d}{\lambda_{\rm D}}\right)^3, \text{ for } \lambda_{\rm D} < d \tag{5}$$

To extend the model to IEMs, *d* should be substituted with fixed charge size as electrostatic effects exerted by the fixed charges are screened by counter- and co-ions. The mean linear distance between fixed charges, *b*, approximates for fixed charge diameter, and eq 5 is rearranged to yield an expression for the reciprocal of screening length:

$$\kappa = \frac{\lambda_{\rm D}^2}{b^3} \tag{6}$$

The Debye length, λ_D , is calculated using eq S11 in the Supporting Information. With eqs 4 and 6, condensed counterion mobilities can be determined using experimentally-accessible characteristics without any adjustable parameters. This model does not distinguish between "territorially" and "site" bound but considers all condensed counterions to be mobile.

MATERIALS AND METHODS

Membranes and Chemicals. Commercial cation and anion exchange membranes (CEM and AEM, respectively), Selemion CMV and Selemion AMV, were purchased from Asahi Glass Co. (Japan). Electrolytes and electrolyte hydrates utilized in the study, NaCl, KCl, NH₄Cl, MgCl₂·6H₂O, CaCl₂·2H₂O, NaBr, Na₂SO₄, MgSO₄·7H₂O, NaNO₃, Na₂CO₃, and Na₃PO₄·12H₂O, were acquired from Thermo Fisher Scientific (Waltham, MA). All salts are reagent grade and used as received to prepare electrolyte solutions. Deionized (DI) water was purified with a Milli-Q ultrapure water purification system (MilliporeSigma, Burlington, MA).

Characterization of Membrane Structural Properties. Ion-exchange capacity, IEC, is the number of fixed charges per unit mass of dry membrane.¹ The IEC of the CEM was determined using the acid titration method, ^{2,41,42} whereas the ion elution method was employed to characterize the AEM.^{37,38,43} Swelling degree, SD, is defined as the mass ratio of sorbed water relative to the dry membrane.¹ As membrane water uptake is influenced by both counterion and external solution concentration, ^{1,12,44} As membrane water uptake is influenced by both counterion and external solution concentration, SD was characterized in 1.0 eq/L of the various electrolyte

solutions investigated in this study (in addition to DI water).³⁷ The contribution of sorbed counterions to the membrane dry mass was accounted for in the determination of IEC and SD.³⁷ Water volume fraction in IEM, f_w , is 12,37,45

$$f_{\rm w} = \frac{\rm SD/\rho_{\rm w}}{\rm SD/\rho_{\rm w} + 1/\rho_{\rm p}} \tag{7}$$

where $\rho_{\rm w}$ and $\rho_{\rm p}$ are the mass density of water and dry membrane polymer, respectively. $\rho_{\rm p}$ of 1.43±0.01 and 1.22±0.01 g/mL, for CMV and AMV, respectively, are taken from our recent study.³⁷ Membrane fixed charge concentration, per unit wet IEM volume, $c_{\rm fix}^{\rm m}$, is^{20,37}

$$c_{\text{fix}}^{\text{m}} = \frac{\text{IEC}}{\text{SD}} f_{\text{w}} \rho_{\text{w}}$$
 (8)

Membrane coupons for all experiments were from the same sheets of CMV and AMV, to minimize potential heterogeneity between samples.

Determination of Membrane Conductivities and Condensed Counterion Mobilities. Ionic conductivities of the IEMs were characterized using the direct current chronopotentiometry method with 1.0 eq/L of different electrolyte solutions in a two-compartment and four-electrode cell system adopting the difference method. Specifically, the CEM was analyzed in NaCl, NaBr, Na₂SO₄, KCl, NH₄Cl, MgCl₂, MgSO₄, and CaCl₂, whereas AEM was evaluated in NaCl, KCl, MgCl₂, NaBr, NaNO₃, Na₂CO₃, Na₂SO₄, MgSO₄, and Na₃PO₄. The relatively high electrolyte concentration of 1.0 eq/L was thoughtfully selected to avoid potential mass transfer limitations in the diffusion boundary layers that may occur at lower concentrations. ^{46–48} Details of the conductivity measurement methodology can be found in our previous studies. ^{37,41,48}

The membrane conductivity, σ_m , can be related to ion concentrations and absolute mobilities in the IEM:^{1,24}

$$\sigma^{\rm m} = \frac{F^2 k_{\rm B}}{R} \left(z_{\rm co}^2 c_{\rm co}^{\rm m} u_{\rm co}^{\rm m} + z_{\rm ct}^2 c_{\rm ct}^{\rm m} \phi_{\rm u} u_{\rm ct, u}^{\rm m} + z_{\rm ct}^2 c_{\rm ct}^{\rm m} \phi_{\rm c} u_{\rm ct, c}^{\rm m} \right)$$
(9)

where F is the Faraday constant and R is the ideal gas constant. Concentrations of counter- and coions within the membrane, $c_{\rm ct}^{\rm m}$ and $c_{\rm co}^{\rm m}$, respectively, are determined by the Donnan-Manning model. ^{14,19,20} Fractions of uncondensed and condensed counterion, $\phi_{\rm u}$ and $\phi_{\rm c}$, respectively, can be computed using eq 1 and $\phi_{\rm u} + \phi_{\rm c} = 1$. $u_{\rm co}^{\rm m}$ and $u_{\rm ct,\,u}^{\rm m}$ are provided by eqs 3 and 2, respectively, and $u_{\rm ct,\,c}^{\rm m}$ are modeled using eqs 4 and 6. All experimental characterizations and model calculations were carried out for T = 298 K. A set of sample calculations to illustrate the modeling of membrane conductivity is provided in the Supporting Information.

RESULTS AND DISCUSSION

The Current Donnan-Manning Transport Model Underestimates Membrane Conductivity. Figure 2 compares the ionic conductivities, σ^m , between experimental measurements and model predictions of the current Donnan-Manning transport model, i.e., assuming condensed counterions are immobile, for the CEM and AEM in various electrolyte solutions. Experimental conductivities of the IEMs are represented by orange hatched columns, with labels above the columns indicating the counterion (complete data is listed in Table S1 of the Supporting Information). The membranes show dissimilar conductivities with different counterions but exhibit indistinguishable conductivities when co-ions are varied with the same counterion. This signifies that IEM conductivity is dominated by counterions.

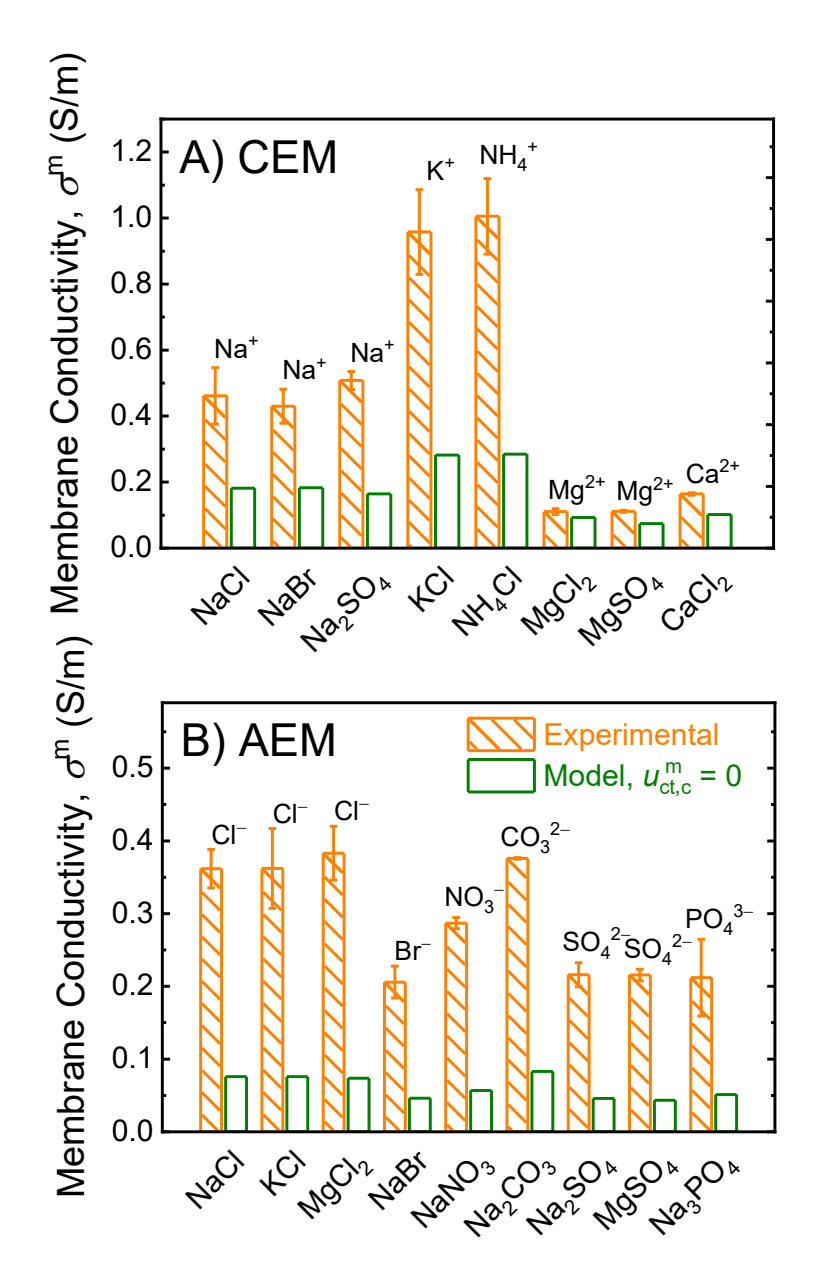


Figure 2. Comparison of membrane conductivities, σ^{m} , between experimental measurements (orange hatched columns) and predictions by the original Donnan-Manning transport model with $u_{ct,c}^{m} = 0$ (green open columns) for A) CEM and B) AEM in different electrolytes. Labels above the columns denote counterions. Note the different vertical axis scales on the plots.

Model IEM conductivities are determined using eq 9 and shown as green open columns. Ion concentrations in membrane matrices are obtained with the Donnan-Manning model based on membrane structural information in Tables S2 and S3 of the Supporting Information, and the

distributions between condensed and uncondensed counterions are calculated using eq 1 (ϕ is presented in Figure S1). Absolute mobilities of co-ion and uncondensed counterion in IEM are determined through eqs 3 and 2, respectively (shown in Figures S2 and S3), and condensed counterion mobilities are assumed to be zero, i.e., $u_{\text{ct,c}}^{\text{m}} = 0$. f_{w} utilized in the model is evaluated using ion-specific swelling degrees in 1.0 eq/L of the different electrolyte solutions (Table S3 of the Supporting Information). Membrane conductivities are clearly underpredicted by the existing model, where condensed counterions are assumed to be immobile, for all electrolyte solutions. For instance, the modeled CEM conductivities in Na⁺ are just 35–46% of experimental data and are lower at \approx 31% in K⁺ and NH₄⁺ (Figure 2A). Compared to monovalent Na⁺, the model slightly underpredicts σ ^m of the CEM with divalent counterions by \approx 10–34%. As for the AEM in Figure 2B, the modeled σ ^m in monovalent counterions merely accounts for 19–22% of experimental data for Cl⁻, Br⁻, and NO₃⁻. Similar underpredictions occur with multivalent counterions (20–24% of observed σ ^m in CO₃²⁻, SO₄²⁻, and PO₄³⁻). The discrepancies between experimental and modeling results shown in Figure 2 are consistent with past studies that adopted the $u_{\text{ct,c}}^{\text{m}} = 0$ assumption. ^{15,17}

The Donnan-Manning transport model has been demonstrated to capture ion partitioning and co-ion diffusion coefficient in IEMs reasonably well (the former through activity coefficients). 13,15,19 Thus, the deviations in modeled membrane conductivities from experimental values can be attributed to membrane counterion mobilities, i.e., the second and third terms in the parenthesis of eq 9. As condensed counterions are assumed to be immobile in the current framework, i.e., $u_{\rm ct,c}^{\rm m}=0$, the counterion mobility in membrane is only from the uncondensed portion of counterions (blue arrow in Figure 1). Since the theoretical treatment for uncondensed counterions mobility is identical to co-ions in the Donnan-Manning model (analytical expression for mobilities, eqs 2 and 3, are essentially identical), 16 the modeling of $u_{\rm ct,u}^{\rm m}$ is reliable and not a principal cause of the discrepancies. Therefore, the significant underprediction of experimental $\sigma^{\rm m}$ by the current model strongly suggests that the assumption of immobile condensed counterions is invalid. The fractions of counterions that are condensed, $\phi_{\rm m}$, range between 0.32 and 0.78 for the investigated IEMs across the different electrolytes (Figure S1 of the Supporting Information), which are nontrivial portions of counterions in the membrane. The substantial $\phi_{\rm m}$ signifies that

condensed counterions, if mobile, would be nonnegligible contributions to the membrane conductivity.

Conductivity Predictions for Monovalent Counterions. Figure 3 presents modeled membrane conductivities of the modified Donnan-Manning transport framework with $u_{ct,c}^{m}$ determined by eq 4, i.e., condensed counterions are mobile, and screening lengths simulated using eq 6 ($u_{ct,c}^{m}$ is presented in Figure S4 of the Supporting Information). Contributions of condensed counterions to the modeled σ^{m} are represented by green filled columns, which are stacked on green open columns denoting the contributions of uncondensed counterions and co-ions. The modeled σ^{m} are compared to experimentally measured membrane conductivities of the CEM and AEM in different electrolyte solutions (orange hatched columns). Note that the green open and orange hatched columns are the data of Figure 2, and labels above the columns indicate the counterion. Complete conductivity data is available in Table S4 of the Supporting Information.

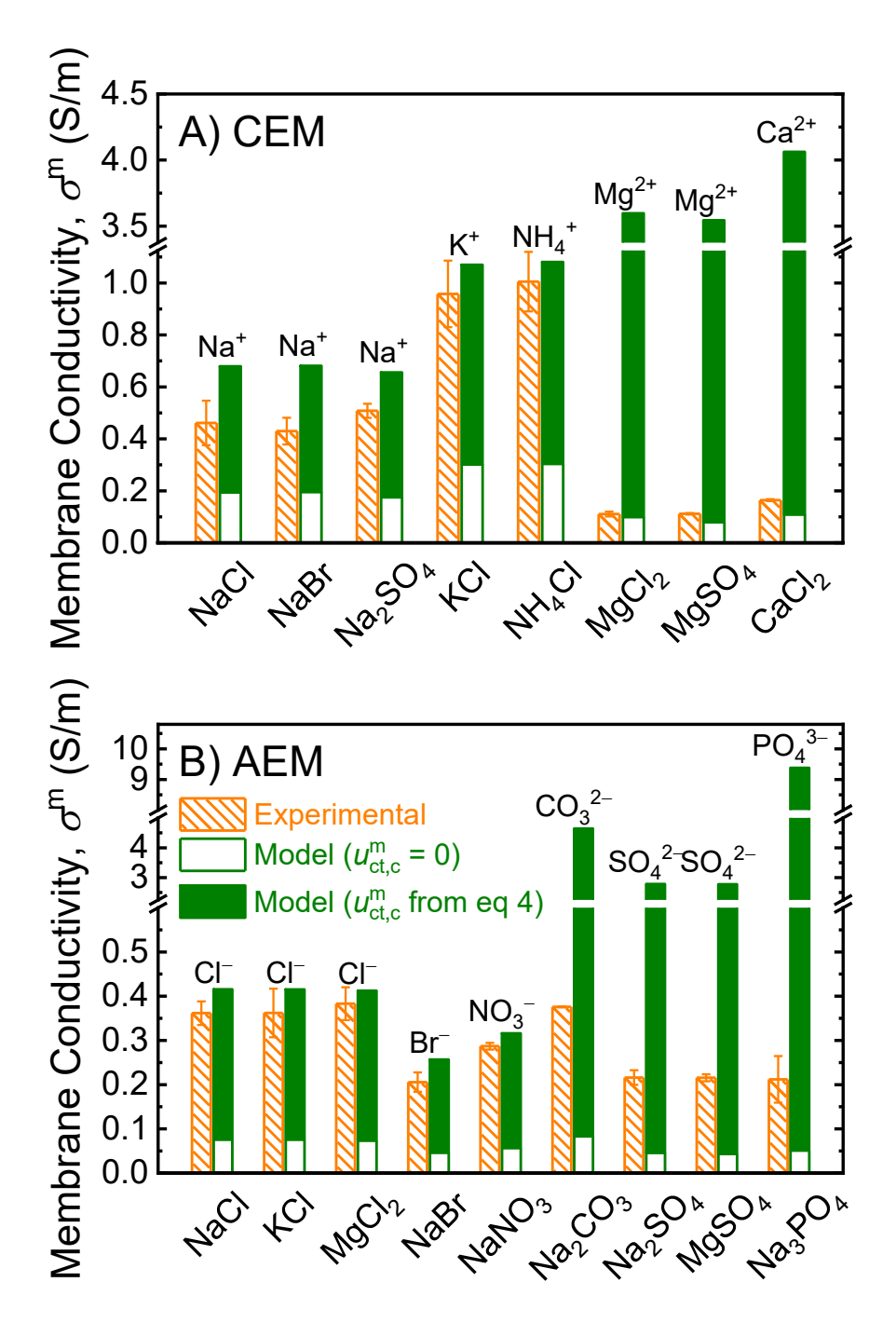


Figure 3. Comparison of membrane conductivities, $\sigma^{\rm m}$, between experimental measurements and model predictions by the Donnan-Manning transport framework for A) CEM and B) AEM in different electrolytes. Experimental observations are denoted by orange hatched columns, whereas green open columns represent the original model with $u_{\rm ct,\,c}^{\rm m}=0$ and stacked green filled columns indicate the contribution of condensed counterions with $u_{\rm ct,\,c}^{\rm m}$ determined using eq 4 (green open and orange hatched columns are

the data of Figure 2). Labels above the columns denote counterions. Note the different scales and breaks on the vertical axes of the plots.

By accounting for the absolute mobilities of condensed counterions, the accuracy of modeled membrane conductivities with monovalent counterions to match with experimental σ^{m} is significantly enhanced. For the AEM (Figure 3B), membrane conductivities of the revised transport model with $u_{\text{cr},c}^{\text{m}}$ from eq 4 are within 0.8–2.3 standard deviations of the experimental characterizations for Cl⁻ and Br⁻ counterions and <4 standard deviations for NO₃⁻. These modeled $\sigma^{\rm m}$ are drastically improved from the sizable underpredictions in Figure 2B, which neglects the mobilities of condensed counterions. The modified model with mobile condensed counterions yields $\sigma^{\rm m}$ for the CEM that are <0.9 standard deviations for K⁺ and NH₄⁺ counterions (Figure 3A), again much better than the gross underpredictions with $u_{ct,c}^{m} = 0$ (Figure 2A). For the CEM with Na⁺ as the counterion, the revised model simulated σ^{m} that are comparatively less accurate than the other monovalent counterions but still represents an increase in overall precision over the old model (29-58% more than experimental observations in Figure 3A, compared to the underpredictions of 54-65% in Figure 2A). Critically, the improvements in accuracy of the modeled membrane conductivities for monovalent counterions are achieved based on first principles and without any adjustable parameters. This highlights the effectiveness of eq 4 to describe the condensed phase mobility and reinforces the validity of the theoretical underpinnings to arrive at the analytical expressions.

The slight overpredictions of membrane conductivities is consistent across all the monovalent counterions investigated and for both CEM and AEM. This could be partly due to enmeshed support layers of the two commercial membranes investigated influencing the experimental $\sigma^{\rm m}$ characterization.⁴⁵ The meshes decrease available free volume and increase tortuosity for ion transport,³⁷ thus lowering the experimentally observed $\sigma^{\rm m}$ relative to pure ion-conducting polymers simulated by the models. Alternatively, the unvarying overpredictions suggest that the assumptions and simplifications adopted may have introduced systemic inaccuracies into the models. The deviations could have stemmed from uncertainties in the original model, ^{12,15,16,18} namely the distribution between condensed and uncondensed counterions, i.e., $\phi_{\rm c}$ (eq 1), uncondensed counterion mobility, $u_{\rm co}^{\rm m}$ (eq 2), and co-ion mobility, $u_{\rm co}^{\rm m}$ (eq 3), or from the

analytical expressions to determine condensed counterion mobility, $u_{\text{ct,c}}^{\text{m}}$, presented in this study (eqs 4–6). For instance, the finite volumes of the charged species, i.e., counterions, co-ions, and fixed charges, are not factored into the models; instead, the entities are considered to be point charges with negligible volume. Accounting for the volumes will decrease the free volume available for ion permeation, and, hence, lower ion mobilities and membrane conductivities. The original counterion condensation theory ignores interactions between polymer chains, a reasonable simplification for relatively dilute polyelectrolyte solutions. But such interactions may play a nonnegligible role in IEMs, which have considerably denser matrices. Additionally, the Debye-Hückel approximation used to treat the co-ions and uncondensed counterions may not be appropriate in the highly charged membrane matrix (as discussed in the Theory section), potentially producing discrepancies in the modeled mobilities of co-ions and uncondensed counterions (and, consequently, σ^{m}).

The revised model produced huge σ^m overpredictions for multivalent counterions. For instance, the modeled CEM conductivities for divalent Mg²⁺ and Ca²⁺ counterions are 25–32× greater than experimental measurements (Figure 3A); whereas in the AEM, the overpredictions are 12–13 fold for divalent CO₃²⁻ and SO₄²⁻ and 44× for trivalent PO₄³⁻ (Figure 3B). For multivalent counterions, the contribution of condensed counterion mobility to net σ^m is \approx 35–183× the contributions from uncondensed counterions and co-ions (green filled columns are much taller than green open columns). Therefore, these large discrepancies are primarily attributed to the modeled condensed phase mobility, implying potential deficiencies in the theoretical framework for multivalent counterions. This will be discussed in a later section, and a potential further modification to the model will be examined.

Monovalent Counterions Are Significantly More Mobile in Condensed Phase than Uncondensed Phase. To deepen the understanding of condensed counterion mobility in IEMs, the relative ion mobilities between condensed, uncondensed, and bulk solution phases are analyzed. Figure 4A displays the mobility ratio of condensed to uncondensed counterions, i.e., $u_{\rm ct,\,c}^{\rm m}/u_{\rm ct,\,u}^{\rm m}$, determined from eqs 4 and 2, respectively, for various electrolytes in the CEM and AEM. Note that only monovalent counterion data is presented as the corresponding membrane conductivity can be modeled with reasonable accuracy (Figure 3).

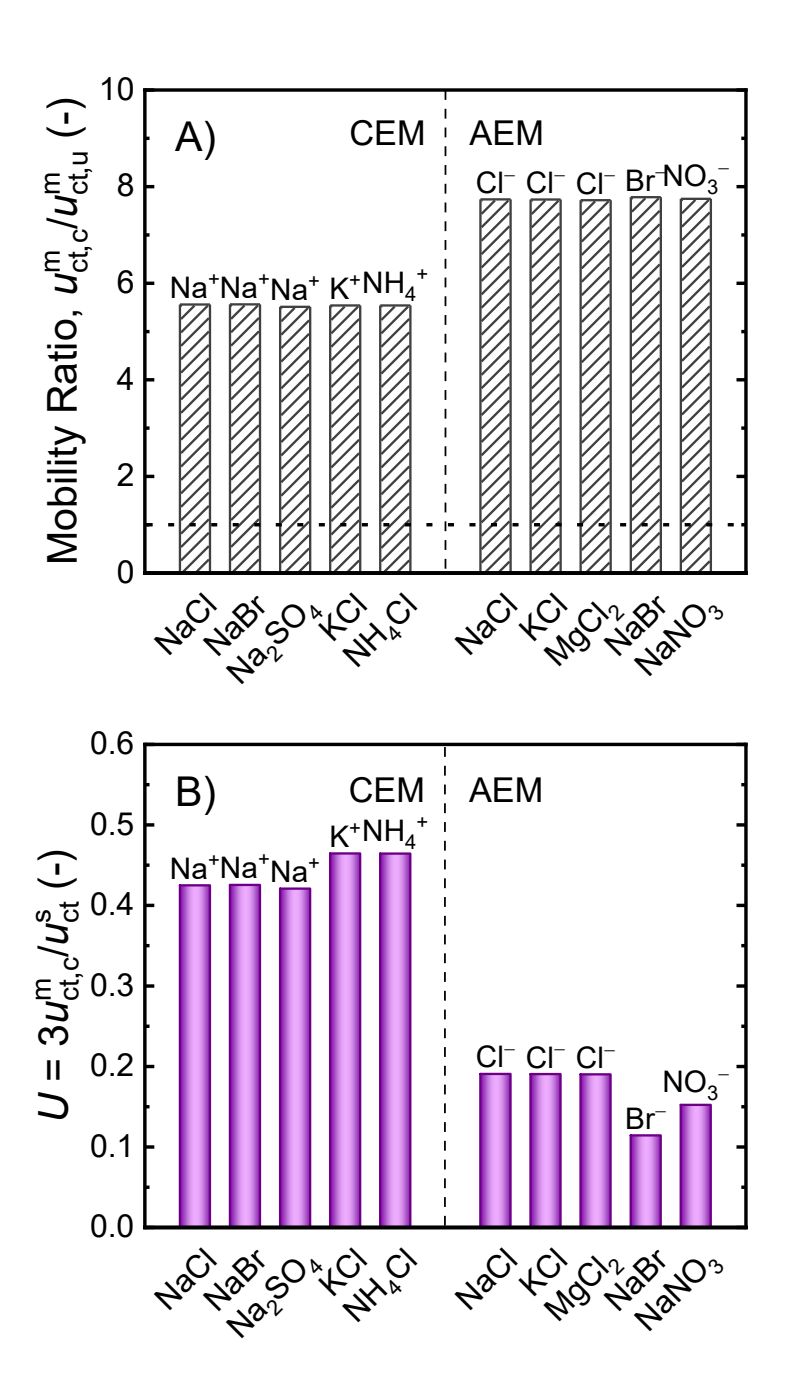


Figure 4. A) Modeled mobility ratios of condensed counterions to uncondensed counterions, $u_{\rm ct,\,c}^{\rm m}/u_{\rm ct,\,u}^{\rm m}$, determined using eqs 4 and 2, respectively. Horizontal dotted line indicates unity. B) $U=3u_{\rm ct,\,c}^{\rm m}/u_{\rm ct}^{\rm s}$, relating condensed counterion mobilities within membranes to bulk phase mobilities in aqueous solutions (factor of 3 accounts for one- and three-dimensional transport in membrane and solution phases, respectively). Labels above

the columns denote counterions. Note that only monovalent counterions are presented as the membrane conductivities can be modeled with reasonable accuracy (Figure 3).

For all the monovalent counterions investigated in the CEM and AEM, counterions show much greater mobility in the condensed phase than in the uncondensed phase, i.e., $u_{\text{ct, c}}^{\text{m}}/u_{\text{ct, u}}^{\text{m}} >> 1$. This is consistent with the experimental results of a past study that looked at IEMs in NaCl solution. Dividing eq 4 by eq 2 yields $u_{\text{ct, c}}^{\text{m}}/u_{\text{ct, u}}^{\text{m}} = \left[1-2\left(|z_{\text{ct}}|\xi-1\right)\ln\left(\kappa b\right)\right]/\left(1-|z_{\text{ct}}|^2A/3\right)$. The $2\left(|z_{\text{ct}}|\xi-1\right)\ln\left(\kappa b\right)$ term in the numerator and the $|z_{\text{ct}}|^2A/3$ term in the denominator represent the effects of electrostatic interactions arising from the fixed charges in the membrane matrix on the mobilities of the condensed and uncondensed counterions, respectively. In the transport framework presented here, condensed and uncondensed counterions have the same permeation pathway, and the spatial factor, $\left[f_{\text{w}}/(2-f_{\text{w}})\right]^2$, in eqs 2 and 4 cancels out in $u_{\text{ct, c}}^{\text{m}}/u_{\text{ct, u}}^{\text{m}}$. Thus, $u_{\text{ct, c}}^{\text{m}}/u_{\text{ct, u}}^{\text{m}} > 1$ signifies that counterions experience less retardation in the condensed phase than in the uncondensed phase.

Further analysis of the terms in $u_{\text{et,e}}^{\text{m}}/u_{\text{et,u}}^{\text{m}}$ reveals insights into counterion mobility within IEMs. In the denominator, $1-|z_{\text{et}}|^2 A/3 < 1$ because the migration of uncondensed counterions is impeded in the rough electric potential resulting from the electrostatic interactions. 16,37,51 For condensed counterions, since $\kappa b << 1$ and $\xi > 1$, $1-2(|z_{\text{et}}|\xi - 1)\ln(\kappa b)$ in the numerator is greater than unity, 30 critically signifying that counterions in the condensed phase are accelerated by the electrostatic interactions. Because the electrostatic interactions have opposite influences on condensed and uncondensed counterions, condensed counterions are considerably more mobile than uncondensed counterions. The results here provide compelling evidence that $u_{\text{et,c}}^{\text{m}} > u_{\text{et,u}}^{\text{m}}$ is universally valid for all monovalent counterions (beyond Na⁺ in CEM and Cl⁻ in AEM). The precise mechanism for the acceleration experienced by condensed counterions is unclear as the analytical expressions of the model do not directly reveal the underlying phenomena. Further investigations are required to elucidate the governing physics. Here, we posit that the local electric potential close to the fixed charges, i.e., influencing condensed counterions, may be different from the local electric potential farther away and affecting uncondensed counterions. If condensed

counterions are on a steeper electric potential gradient, they may be accelerated whereas uncondensed counterions are retarded by a more gentle and undulating gradient.

Notably, the relative mobilities between condensed and uncondensed counterions are very similar across different counter- and co-ions for the CEM and AEM at \approx 5.5 and \approx 7.7, respectively. Because ions are treated as point charges in this theoretical framework, the principal ion property in eqs 2 and 4 is valence. 16,18,30 Hence, $u_{\rm ct,\,c}^{\rm m}/u_{\rm ct,\,u}^{\rm m}$ is essentially the same for the different monovalent counterions (Na⁺, K⁺, and NH₄⁺ for the CEM and Cl⁻, Br⁻, and NO₃⁻ for the AEM). Additionally, the co-ion has negligible influence on $u_{\rm ct,\,c}^{\rm m}/u_{\rm ct,\,u}^{\rm m}$ (mobility ratios for NaCl, NaBr, and Na₂SO₄ in CEM and NaCl, KCl, and MgCl₂ for AEM are almost identical in Figure 4A). For the same membrane, the miniscule $u_{\rm ct,\,c}^{\rm m}/u_{\rm ct,\,u}^{\rm m}$ variations (< 0.4%) between the different counterand co-ions are due to marginally dissimilar $c_{\rm co}^{\rm m}$ and ionic strength within the IEM (and also different $z_{\rm co}$ and $v_{\rm co}$ for co-ions of unlike valences). On the other hand, the difference in overall mobility ratios between the CEM and AEM (i.e., \approx 5.5 and \approx 7.7, respectively) is mainly attributed to the distinct properties of each membrane, specifically $c_{\rm fix}^{\rm m}$, ξ , and b.

Counterion Mobility is Lower in Condensed Phase than in Bulk Solution Phase Because Spatial Impediment Outweighs Electrostatic Acceleration. The condensed counterion mobility can be related to the ion mobility in bulk solution with the expression $u_{ct,c}^{\rm m} = Uu_{ct}^{\rm s}/3$. ^{14,15} The factor of 1/3 accounts for transport of condensed counterions along the polymer backbone in the same direction as effective transmembrane ion flux, rather than in the other two orthogonal directions. Thus, U > 1 and < 1 indicate that the ion in condensed phase has larger and smaller mobilities, respectively, than in bulk solution phase, with U reflecting the net aggregated outcome of various effects on condensed counterions migration within the IEM matrix (e.g., electrical, structural, and chemical interactions between the condensed counterions and the functional groups, polymer backbone, and water molecules). Figure 4B compares $U = 3u_{ct,c}^{\rm m}/u_{ct}^{\rm s}$ for different condensed counterions in CEM and AEM, with $u_{ct,c}^{\rm m}$ determined using eq 4 and $u_{ct}^{\rm s}$ from literature data⁸. Again, only results of monovalent counterions are shown.

For all monovalent counterions investigated in the CEM and AEM, U is less than unity, signifying that counterions condensed along the membrane polymer chains have impeded

mobilities relative to ions in the bulk solution. This result is consistent with previous postulations. 15,17 U varies among different counterions for the CEM and AEM (for instance, U is ≈ 0.42 for Na⁺ and ≈ 0.46 for K⁺ and NH₄⁺ in the CEM), but co-ion identity has no significant influence on U (e.g., U of Na+ in CEM is essentially invariant despite different co-ions). These trends can be explained within the framework of condensed counterion mobility. Substituting $u_{\text{ct, c}}^{\text{m}} = U u_{\text{ct}}^{\text{s}} / 3$ into eq 4 gives $U = 3 \left[f_{\text{w}} / (2 - f_{\text{w}}) \right]^2 \left[1 - 2 \left(\left| z_{\text{ct}} \right| \xi - 1 \right) \ln \left(\kappa b \right) \right]$. For different monovalent counterions in the same membrane, the electrostatic terms, $[1-2(|z_{ct}|\xi-1)\ln(\kappa b)]$, are highly similar since parameters of the term, ξ , κ , and b, are chiefly determined by membrane properties (and $|z_{ct}| = 1$). Hence, U of different monovalent counterions is primarily differentiated by the spatial term, $\left[f_{\rm w}/(2-f_{\rm w})\right]^2$, which is dependent on the water volume fraction, f_w . Because f_w is influenced by the electrolyte, the spatial term varies across the different counterions examined here. Experimentally characterized f_w of the CEM are $K^+ \approx NH_4^+ > Na^+$ (Table S3 of the Supporting Information), consistent with the magnitude order of U in Figure 4B. Likewise for the AEM, f_w from swelling degree characterizations account for the trend in $U: Cl^- >$ $NO_3^- > Br^-$. In contrast, none of the critical factors, i.e., f_w , ξ , κ , and b, is sensitive to co-ion identity. Thus, U is almost indistinguishable between different co-ions for counterions of Na $^+$ in CEM and Cl⁻ in AEM (the minute disparities in U of < 0.6% is because c_{co}^{m} and ionic strength within the IEMs are not exactly identical).

Overall, mobilities of condensed monovalent counterions are more suppressed in the AEM, with U of 0.11–0.19 significantly lower than 0.42–0.46 of the CEM. U is principally influenced by membrane properties f_w , ξ , κ , and b (as discussed above). The gap in U is, thus, because of dissimilar intrinsic properties between the two membranes. Due to lower κb and larger ξ , the electrostatic terms for the AEM investigate here are slightly larger than the CEM, i.e., condensed counterions experience greater acceleration from the electrostatic effect in the AEM relative to the CEM. However, AEM water uptake is much lower than the CEM, reducing the available volume for ion permeation and increasing the tortuosity of the transport pathway. Overall, the spatial effect overwhelms the electrostatic effect for the two IEMs studied here, and U of the AEM is less than half of the CEM (parameters f_w , ξ , κ , and b and calculated values of the spatial and electrostatic terms are summarized in Tables S2, S3, and S5 of the Supporting Information). As only one CEM

and AEM each are examined in this study under a limited set of operation conditions, further investigations to include membranes with distinctly different characteristics and a wider range of operation conditions (e.g., different bulk solution concentrations) are recommended to more rigorously probe the generalizability of these observations.

Poor Predictions for Multivalent Counterions Can be Attributed to Gaps in Fundamental Physics Describing Screening Length of Ion-Ion Interactions. The large overpredictions for multivalent counterions given by the condensed counterion mobility framework presented here (earlier discussion of Figure 3) could be due to inadequacy of the screening length scaling relationship for multivalent ions. The equation for the screening length scaling relationship, eq 5, is based on experiments with only monovalent electrolytes, i.e., multivalent ions were not studied. 32,35,36 Therefore, applying the relationship to multivalent ions in this analysis could have overextended its applicability.

From a further analysis of the applicability of the screening length scaling relationship (presented in the Supporting Information), we conjecture that the exponent of the power law scaling relationship (eq 5) for multivalent ions is different from monovalent ions. Using a power law exponent of 1 (rather than 3 in eq 5), as informed by the analysis (Table S6 in the Supporting Information), the screening length scaling relationship for multivalent ions can be expressed instead as $(\kappa \lambda_D)^{-1} = d/\lambda_D$. Modeled membrane conductivities, σ^m , of the CEM and AEM for multivalent counterions utilizing the revised exponent of 1 are presented in Figure 5 and compared against the experimental measurements (blue filled and orange hatched columns, respectively. Labels above the columns are the modeled σ^m using the original power law exponent of 3 (i.e., eq 5 and model results of Figure 3). Note that MgCl₂ in CEM and MgSO₄ in AEM were analyzed but not included in Figure 5 because the results are practically identical to MgSO₄ and Na₂SO₄, respectively (results for MgCl₂ in CEM and MgSO₄ in AEM can be found in Figure S6 of the Supporting Information).

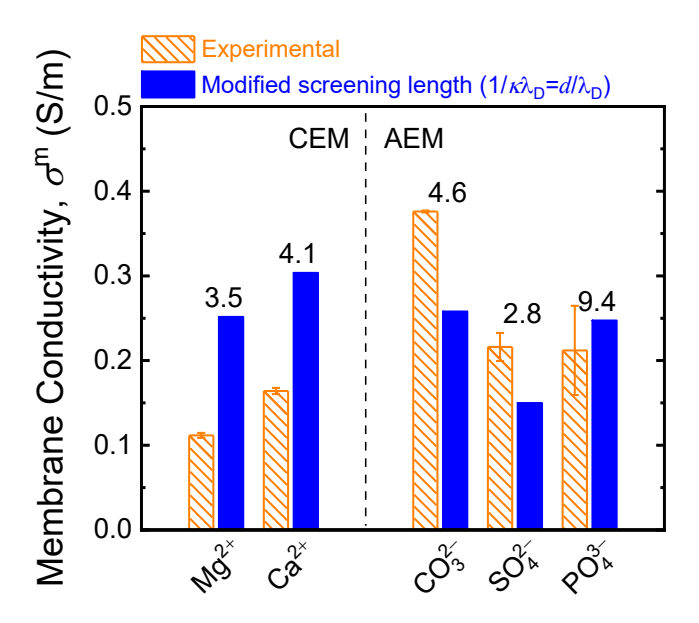


Figure 5. Comparison of membrane conductivities, σ^{m} , between experimental measurements and modified model predictions (orange hatched and blue filled columns, respectively) for multivalent counterions in the CEM and AEM. The power law exponent of the screening length scaling relationship, eq 5, is modified to 1 for the multivalent ions (from the original 3), i.e., $(\kappa\lambda_{D})^{-1} = d/\lambda_{D}$ instead of $(d/\lambda_{D})^{3}$. Labels above the columns indicate modeled σ^{m} using the original power law exponent of 3 (model results of Figure 3). Electrolytes for the CEM are MgSO₄ and CaCl₂, whereas electrolytes for the AEM are Na₂CO₃, Na₂SO₄, and Na₃PO₄.

Modifying the power law exponent of the screening length scaling relationship significantly improves model accuracy of membrane conductivities for multivalent counterions. For instance, the modified model yields AEM conductivities -31 to 17% of the experimental observations for counterions CO_3^{2-} , SO_4^{2-} , and PO_4^{3-} , a substantial improvement over the large overpredictions of $12-44\times$ with the original power law. Similarly, modeled σ^m using the adjusted power law exponent are only around 85-125% higher than the CEM experimental conductivities in divalent counterions of Mg^{2+} and Ca^{2+} , considerably enhanced compared to the initial $25-32\times$ overpredictions. The analysis provides evidence that the screening length scaling relationship presented in eq 5 is likely not valid for multivalent ions. Further, the results suggest that the condensed phase mobility of multivalent counterions can be better described by a modification to the power law exponent of the screening length scaling relationship. The proposed modification

of $(\kappa \lambda_D)^{-1} = d/\lambda_D$ further simplifies to $\kappa = 1/d$ and λ_D vanishes, signifying that κ is independent of concentration for multivalent ions in the high concentration range. As the modification is based on quantitative analysis of the empirical data (Table S6 of the Supporting Information) and not derived from first principles,_further investigations of the electrostatic screening length in concentrated multivalent electrolyte solutions will be needed to establish a more rigorous expression for the screening length and elucidate the fundamental role of ion valence. Moreover, with $\kappa = 1/d = 1/b$, the electrostatic term in eq 4 collapses to unity for condensed multivalent counterions, signifying that ions are not accelerated by the electrostatic effect like condensed monovalent counterions, and $u_{\rm ct,c}^{\rm m}$ of multivalent species are only influenced by the spatial effect in the modified model. Because multivalent counterions in the condensed phase are also not retarded by the electrostatic effect like ions in the uncondensed phase $(1-|z|^2 A/3 < 1, {\rm eq} 2)$, $u_{\rm ct,c}^{\rm m}$ are still greater than $u_{\rm ct,u}^{\rm m}$ for multivalent counterions (spatial effects are identical in both phases).

Membrane Conductivities are More Accurately Described with Model Modifications. Figure 6 compares the accuracy of modeled membrane conductivities without and with the contributions of condensed phase mobility, i.e., the current Donnan-Manning model and the modified transport framework presented in this study, respectively. In Figure 6A, σ^{m} s of the CEM and AEM (blue circle and red square symbols, respectively) modeled by the original transport framework with $u_{ct,c}^{m} = 0$ are compared against experimental membrane conductivities in various electrolytes. The parity plot shows that all conductivities are underpredicted by the present model and many are substantially below the experimentally observed σ^{m} (as discussed in detail earlier for Figure 2).

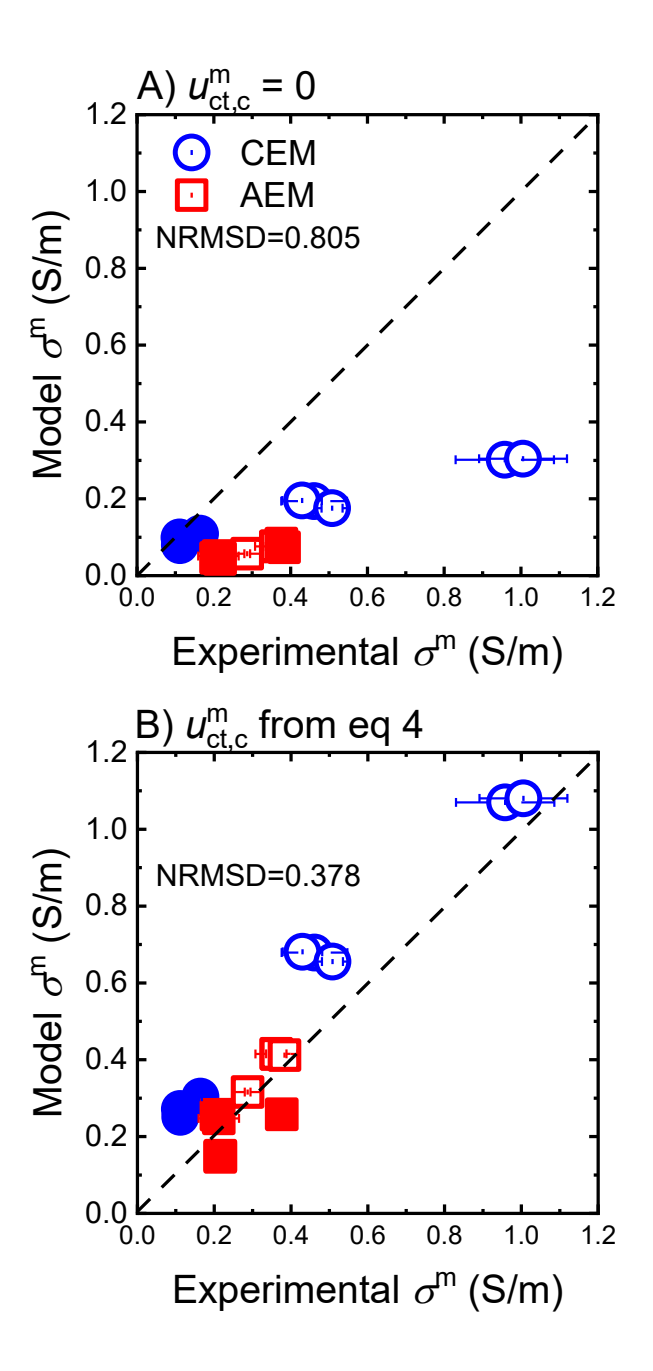


Figure 6. Parity plots comparing membrane conductivities, σ^m , from experimental measurements and model predictions by the Donnan-Manning transport framework in different electrolytes. A) Model σ^m is determined by the original Donnan-Manning transport model with $u_{ct,c}^m = 0$. B) Model σ^m is evaluated using the modifications to the theoretical framework presented here, namely: i) $u_{ct,c}^m$ is determined by accounting for electrostatic interactions and spatial effects on condensed counterions (eq 4), ii) screening length experienced by monovalent counterions is expressed by eqs 5 and 6, and iii)

screening length for multivalent counterions is described by the modified power law relationship of $(\kappa\lambda_D)^{-1} = (d/\lambda_D)$. CEM and AEM are denoted by blue circle and red square symbols, respectively. Monovalent, divalent, and trivalent counterions are open, partially transparent filled, and solid symbols, respectively. Calculation method for the normalized root-mean-square deviation, NRMSD, is detailed in the Supporting Information.

Figure 6B presents the same comparison but with the contribution of condensed counterions included in the modeled σ^m , i.e., $u_{ct,c}^m$ is determined using eq 4. The screening length relationship of eq 5 is utilized for monovalent counterions (open symbols), whereas the modified power law relationship of $(\kappa\lambda_D)^{-1} = (d/\lambda_D)$ is adopted for multivalent counterions (partially transparent filled and solid symbols for divalent and trivalent counterions, respectively). Accounting for condensed counterion mobility drastically improves the accuracy of the modified transport model to predict membrane conductivity. Normalized root-mean-square deviation, NRMSD, statistically quantifies the differences between observed and predicted values (calculation method is detailed in the Supporting Information). Solventh RMSD of the modified model is 0.378, largely improved from 0.805 of the original transport model that ignores $u_{ct,c}^m$ (residual analysis for the current and modified models is presented in Figure S7 of the Supporting Information). This reinforces the critical contribution of mobile condensed counterions to IEM transport and underlines the effectiveness of the modified condensed counterion mobility framework in improving the quantitative description of membrane conductivity.

IMPLICATIONS

This study presents a model to express the mobility of condensed counterions in IEMs using an analytical equation (eq 4). Conventional theories for electrolyte chemistry, such as the Debye-Hückel theory, are unable to describe the screening length in highly charged membrane matrices, breaking down when the Debye length is smaller than the ion diameter. The novel introduction of a scaling relationship overcame this limitation. The current Donnan-Manning transport model underestimates the membrane conductivities, sometimes by as much as a factor of 5, because the condensed counterion mobility is neglected. After incorporating the contributions of condensed counterions using the screening length scaling relationship, accuracy of the modeled IEM

conductivities is significantly enhanced for monovalent counterions. Critically, the modified framework does not employ any adjustable parameters, i.e., the membrane conductivities can be determined *a priori*. Further analysis indicates that monovalent counterions are much more mobile in the condensed phase than in the uncondensed phase. This is because electrostatic interactions have opposite influences on condensed and uncondensed counterions: uncondensed counterions are retarded whereas condensed counterions are accelerated. But due to the hindrance caused by the spatial effect, condensed monovalent counterions are less mobile in the membrane than in bulk solution. The modified model is able to achieve reasonable precision in predicting membrane conductivities for multivalent counterions after further adjusting the power law exponent of the screening length scaling relationship.

The proposed revision to the screening length power law is based on our relatively simple analysis. Future experimental investigations and theory development are needed to more robustly extend the screening length scaling relationship to multivalent ions in high ionic strength environments.^{32,35} Deepening the understanding of screening length in highly charged systems and elucidating the role of ion valence can further improve the transport models and shed light on the counterion condensation phenomenon. In addition to electrostatic interactions and spatial effects, other factors such as molecular frictions between mobile ions,⁵³ ion-polymer backbone interactions, ⁵⁴ and ion pairing, ⁵⁵ may also influence ion mobility and transport. These factors are not included in the transport framework of this study and could possibly explain some of the discrepancies between model and experimental conductivities. Some assumptions adopted in the current framework, such as homogeneous membrane matrix and negligible ion size, simplified the modeling and enabled transport to be described using analytical expressions. However, imprecisions may have crept into the model through the simplifying assumptions and warrants further examination. Formulating a more complete ion transport framework for IEMs can provide key insights on membrane structure-property-performance relationships and inform the rational development of better membranes.

The findings of the present study have important implications for improving IEMs. Because condensed counterions are more mobile (accelerated by the electrostatic effect) than uncondensed counterions (retarded), the development of membranes that condense a larger fraction of counterions would yield enhanced conductivities. Selective separations between ions with the same valence are needed for water, energy, and environmental applications, e.g.,

removing Pb²⁺ from Ca²⁺ and Mg²⁺ in drinking water, isolating Li⁺, a critical material for energy, from Na⁺ and K⁺ in geothermal brines, and recovering nutrients NO₃⁻, NH₄⁺, and H_xPO₄^{x-3} from wastewaters containing other ions. 56-58 Conventional IEMs with ion transport governed by the framework investigated here are unlikely to achieve strong migration differentiation between counterions of the same valence. This is because relative ion mobility in the membrane does not significantly change compared to the ratio in bulk solution, which is typically within a factor of 1. Overall selectivity is the product of sorption and migration selectivities. 9,59,60 Therefore, strategies to enhance the discrimination between like-valence ions will have to target sorption selectivity. Robust mechanistic models that accurately simulate sorption for systems with multiple counterions can be integrated with the ion mobility theories in this study to form a unified transport framework and guide the rational development of tailored membranes for ion-specific separations. However, current analytical models for counterion sorption (including the Donnan-Manning model) fall short in multi-ion systems and are, thus, confined to single binary electrolytes (i.e., M^{m+} and X^{x-} only). ¹⁴ Progress was made in a recent study that demonstrated more exact predictions for mixed electrolytes, but the model required an empirical fitting parameter. ⁶¹ Thus, further research efforts are needed to achieve a first principle-based transport framework for accurate transport modeling of multi-ion systems. Other mechanisms, such as coordination chemistry, precise size sieving, and ion intercalation in inorganic materials, can also be leveraged for specific ion-selectivity.9

ASSOCIATED CONTENT

572

573

574

575

576

577

578579

580

581

582

583

584

585

586

587

588

589

590

591

592

593

594

595

596

597

598

599

Supporting Information. The Supporting Information is available free of charge at https://pubs.acs.org/doi/10.1021/acs.estlett.xxxxxxx.

Derivation of analytical expression for condensed counterion mobility, analysis of deviations between model predictions and experiment observations, illustrative calculations modeled membrane conductivity, IEM properties (ion-exchange capacity, polymer density, Manning parameter, mean intercharge distance, swelling degree, and water volume fraction), experimental and modeled membrane conductivities, condensed counterion fractions, modeled ion mobilities, contributions of spatial and electrostatic effects to condensed counterion mobility, analysis of the screening length scaling relationship for multivalent counterions.

ACKNOWLEDGEMENTS

- The authors are grateful to Dr. Alpha Lee (Harvard University) and Dr. Susan Perkins (University)
- of Oxford) for the insightful technical discussions on the screening length scaling relationship.
- This material is based upon work supported by the National Science Foundation under Grant No.
- 604 2207238. Any opinions, findings, and conclusions or recommendations expressed in this material
- are those of the author(s) and do not necessarily reflect the views of the National Science
- 606 Foundation.

600

607

REFERENCES

- 608 (1) Strathmann, H. Ion-Exchange Membrane Separation Processes; Elsevier, 2004.
- 609 (2) Sata, T. *Ion Exchange Membranes: Preparation, Characterization, Modification and Application*; The Royal Society of Chemistry: Cambridge, 2004.
- 611 (3) Xu, T. Ion Exchange Membranes: State of Their Development and Perspective. *Journal of Membrane Science* **2005**, *263* (1–2), 1–29. https://doi.org/10.1016/j.memsci.2005.05.002.
- 613 (4) Strathmann, H. Electrodialysis, a Mature Technology with a Multitude of New Applications.

 614 Desalination 2010, 264 (3), 268–288. https://doi.org/10.1016/j.desal.2010.04.069.
- 615 (5) Strathmann, H.; Grabowski, A.; Eigenberger, G. Ion-Exchange Membranes in the Chemical Process Industry. *Ind. Eng. Chem. Res.* **2013**, *52* (31), 10364–10379. https://doi.org/10.1021/ie4002102.
- 618 (6) Ran, J.; Wu, L.; He, Y.; Yang, Z.; Wang, Y.; Jiang, C.; Ge, L.; Bakangura, E.; Xu, T. Ion 619 Exchange Membranes: New Developments and Applications. *Journal of Membrane Science* 620 **2017**, *522*, 267–291. https://doi.org/10.1016/j.memsci.2016.09.033.
- 621 (7) Epsztein, R.; DuChanois, R. M.; Ritt, C. L.; Noy, A.; Elimelech, M. Towards Single-Species 622 Selectivity of Membranes with Subnanometre Pores. *Nat. Nanotechnol.* **2020**, *15* (6), 426– 623 436. https://doi.org/10.1038/s41565-020-0713-6.
- (8) Luo, T.; Abdu, S.; Wessling, M. Selectivity of Ion Exchange Membranes: A Review.
 Journal of Membrane Science 2018, 555, 429–454.
 https://doi.org/10.1016/j.memsci.2018.03.051.
- (9) Fan, H.; Huang, Y.; Yip, N. Y. Advancing Ion-Exchange Membranes to Ion-Selective
 Membranes: Principles, Status, and Opportunities. Front. Environ. Sci. Eng. 2022, 17 (2), 25.
 https://doi.org/10.1007/s11783-023-1625-0.
- 630 (10) Kamcev, J.; Freeman, B. D. Charged Polymer Membranes for Environmental/Energy 631 Applications. *Annual Review of Chemical and Biomolecular Engineering* **2016**, 7 (1), 111– 632 133. https://doi.org/10.1146/annurev-chembioeng-080615-033533.
- 633 (11) Sujanani, R.; Landsman, M. R.; Jiao, S.; Moon, J. D.; Shell, M. S.; Lawler, D. F.; Katz, L. E.; Freeman, B. D. Designing Solute-Tailored Selectivity in Membranes: Perspectives for
- Water Reuse and Resource Recovery. *ACS Macro Lett.* **2020**, *9* (11), 1709–1717.
- https://doi.org/10.1021/acsmacrolett.0c00710.

- 637 (12) Kamcev, J.; Paul, D. R.; Freeman, B. D. Ion Activity Coefficients in Ion Exchange 638 Polymers: Applicability of Manning's Counterion Condensation Theory. *Macromolecules* 639 **2015**, 48 (21), 8011–8024. https://doi.org/10.1021/acs.macromol.5b01654.
- (13) Kamcev, J.; Paul, D. R.; Manning, G. S.; Freeman, B. D. Predicting Salt Permeability
 Coefficients in Highly Swollen, Highly Charged Ion Exchange Membranes. ACS Appl Mater
 Interfaces 2017, 9 (4), 4044–4056. https://doi.org/10.1021/acsami.6b14902.
- (14) Kitto, D.; Kamcev, J. Manning Condensation in Ion Exchange Membranes: A Review on
 Ion Partitioning and Diffusion Models. *Journal of Polymer Science* 2022, 1–45.
 https://doi.org/10.1002/pol.20210810.
- (15) Kamcev, J.; Paul, D. R.; Manning, G. S.; Freeman, B. D. Ion Diffusion Coefficients in
 Ion Exchange Membranes: Significance of Counterion Condensation. *Macromolecules* 2018,
 51 (15), 5519–5529. https://doi.org/10.1021/acs.macromol.8b00645.
- 649 (16) Manning, G. S. Limiting Laws and Counterion Condensation in Polyelectrolyte Solutions 650 II. Self-Diffusion of the Small Ions. *J. Chem. Phys.* **1969**, *51*, 934–938.
- (17) Wang, Q.; Chen, G. Q.; Kentish, S. E. Sorption and Diffusion of Organic Acid Ions in
 Anion Exchange Membranes: Acetate and Lactate Ions as a Case Study. *Journal of Membrane Science* 2020, 614, 118534. https://doi.org/10.1016/j.memsci.2020.118534.
- (18) Manning, G. S. Limiting Laws and Counterion Condensation in Polyelectrolyte Solutions
 I. Colligative Properties. *J Chem Phys* 1969, 51 (19), 924–933.
 https://doi.org/10.1063/1.1701839.
- (19) Kamcev, J.; Galizia, M.; Benedetti, F. M.; Jang, E. S.; Paul, D. R.; Freeman, B. D.;
 Manning, G. S. Partitioning of Mobile Ions between Ion Exchange Polymers and Aqueous
 Salt Solutions: Importance of Counter-Ion Condensation. *Phys Chem Chem Phys* 2016, 18
 (8), 6021–6031. https://doi.org/10.1039/c5cp06747b.
- (20) Fan, H.; Yip, N. Y. Elucidating Conductivity-Permselectivity Tradeoffs in Electrodialysis
 and Reverse Electrodialysis by Structure-Property Analysis of Ion-Exchange Membranes.
 Journal of Membrane Science 2019, 573, 668–681.
 https://doi.org/10.1016/j.memsci.2018.11.045.
- (21) Kamcev, J. Ion Sorption and Transport in Ion Exchange Membranes Importance of
 Counter-Ion Condensation, The University of Texas at Austin, 2016, Vol. Doctor of
 Philosophy.
- Mackie, J. S.; Meares, P.; Rideal, E. K. The Diffusion of Electrolytes in a Cation Exchange Resin Membrane I. Theoretical. *Proceedings of the Royal Society of London.* Series A. Mathematical and Physical Sciences 1955, 232 (1191), 498–509.
 https://doi.org/10.1098/rspa.1955.0234.
- (23) Mackie, J. S.; Meares, P.; Rideal, E. K. The Diffusion of Electrolytes in a Cation Exchange Resin Membrane. II. Experimental. *Proceedings of the Royal Society of London.* Series A. Mathematical and Physical Sciences 1955, 232 (1191), 510–518.
 https://doi.org/10.1098/rspa.1955.0235.
- 676 (24) Bard, A. J.; Faulkner, L. R. *Electrochemical Methods: Fundamentals and Applications*, 677 2nd ed.; Wiley: New York, 2001.
- 678 (25) Robinson, R. A.; Stokes, R. H. *Electrolyte Solutions*; Courier Corporation, 2002.

- (26) Bordi, F.; Cametti, C.; Colby, R. H. Dielectric Spectroscopy and Conductivity of
 Polyelectrolyte Solutions. *J. Phys.: Condens. Matter* **2004**, *16* (49), R1423–R1463.
 https://doi.org/10.1088/0953-8984/16/49/R01.
- 682 (27) Manning, G. S. A Condensed Counterion Theory for Polarization of Polyelectrolyte 683 Solutions in High Fields. *The Journal of Chemical Physics* **1993**, *99* (1), 477–486. 684 https://doi.org/10.1063/1.465772.
- 685 (28) Manning, G. S. Counterion Binding in Polyelectrolyte Theory. *Accounts of Chemical Research* **1979**, *12* (12), 443–449.
- 687 (29) Luo, H.; Agata, W.-A. S.; Geise, G. M. Connecting the Ion Separation Factor to the 688 Sorption and Diffusion Selectivity of Ion Exchange Membranes. *Ind. Eng. Chem. Res.* **2020**, 689 59 (32), 14189–14206. https://doi.org/10.1021/acs.iecr.0c02457.
- 690 (30) Manning, G. S. A Counterion Condensation Theory for the Relaxation, Rise, and
 691 Frequency Dependence of the Parallel Polarization of Rodlike Polyelectrolytes. *Eur. Phys. J.*692 E 2011, 34 (4), 39. https://doi.org/10.1140/epje/i2011-11039-2.
- (31) Manning, G. S. Counterion Condensation Theory Constructed from Different Models.
 Physica A: Statistical Mechanics and its Applications 1996, 231 (1), 236–253.
 https://doi.org/10.1016/0378-4371(95)00452-1.
- 696 (32) Smith, A. M.; Lee, A. A.; Perkin, S. The Electrostatic Screening Length in Concentrated Electrolytes Increases with Concentration. *J. Phys. Chem. Lett.* **2016**, 7 (12), 2157–2163. https://doi.org/10.1021/acs.jpclett.6b00867.
- 699 (33) Penafiel, L. M.; Litovitz, T. A. High Frequency Dielectric Dispersion of Polyelectrolyte 700 Solutions and Its Relation to Counterion Condensation. *The Journal of Chemical Physics* 701 **1992**, *97* (1), 559–567. https://doi.org/10.1063/1.463604.
- 702 (34) Nightingale, E. R. Phenomenological Theory of Ion Solvation. Effective Radii of Hydrated Ions. *J. Phys. Chem.* **1959**, *63* (9), 1381–1387. 704 https://doi.org/10.1021/j150579a011.
- 705 (35) Lee, A. A.; Perez-Martinez, C. S.; Smith, A. M.; Perkin, S. Scaling Analysis of the Screening Length in Concentrated Electrolytes. *Phys. Rev. Lett.* **2017**, *119* (2), 026002. https://doi.org/10.1103/PhysRevLett.119.026002.
- 708 (36) A. Lee, A.; S. Perez-Martinez, C.; M. Smith, A.; Perkin, S. Underscreening in Concentrated Electrolytes. *Faraday Discussions* **2017**, *199* (0), 239–259. 710 https://doi.org/10.1039/C6FD00250A.
- 711 (37) Fan, H.; Huang, Y.; Billinge, I. H.; Bannon, S. M.; Geise, G. M.; Yip, N. Y. Counterion 712 Mobility in Ion-Exchange Membranes: Spatial Effect and Valency-Dependent Electrostatic 713 Interaction. *ACS EST Eng.* **2022**, *2* (7), 1274–1286. 714 https://doi.org/10.1021/acsestengg.1c00457.
- 715 (38) Dlugolecki, P.; Nymeijer, K.; Metz, S.; Wessling, M. Current Status of Ion Exchange 716 Membranes for Power Generation from Salinity Gradients. *Journal of Membrane Science* 717 **2008**, *319* (1–2), 214–222. https://doi.org/10.1016/j.memsci.2008.03.037.
- 718 (39) Gaddam, P.; Ducker, W. Electrostatic Screening Length in Concentrated Salt Solutions. 719 *Langmuir* **2019**, *35* (17), 5719–5727. https://doi.org/10.1021/acs.langmuir.9b00375.

- (40) Gebbie, M. A.; Dobbs, H. A.; Valtiner, M.; Israelachvili, J. N. Long-Range Electrostatic
 Screening in Ionic Liquids. *Proc Natl Acad Sci USA* 2015, *112* (24), 7432–7437.
 https://doi.org/10.1073/pnas.1508366112.
- 723 (41) Fan, H.; Huang, Y.; Yip, N. Y. Advancing the Conductivity-Permselectivity Tradeoff of Electrodialysis Ion-Exchange Membranes with Sulfonated CNT Nanocomposites. *Journal of Membrane Science* **2020**, *610*, 118259. https://doi.org/10.1016/j.memsci.2020.118259.
- 726 (42) Güler, E.; Elizen, R.; Vermaas, D. A.; Saakes, M.; Nijmeijer, K. Performance-727 Determining Membrane Properties in Reverse Electrodialysis. *Journal of Membrane Science* 728 **2013**, 446, 266–276. https://doi.org/10.1016/j.memsci.2013.06.045.
- 729 (43) Ji, Y.; Luo, H.; Geise, G. M. Effects of Fixed Charge Group Physicochemistry on Anion 730 Exchange Membrane Permselectivity and Ion Transport. *Phys Chem Chem Phys* **2020**, *22* 731 (14), 7283–7293. https://doi.org/10.1039/d0cp00018c.
- 732 (44) Chen, G. Q.; Wei, K.; Hassanvand, A.; Freeman, B. D.; Kentish, S. E. Single and Binary 733 Ion Sorption Equilibria of Monovalent and Divalent Ions in Commercial Ion Exchange 734 Membranes. *Water Research* **2020**, *175*, 115681. 735 https://doi.org/10.1016/j.watres.2020.115681.
- 736 (45) Kingsbury, R. S.; Zhu, S.; Flotron, S.; Coronell, O. Microstructure Determines Water and Salt Permeation in Commercial Ion-Exchange Membranes. *ACS Appl. Mater. Interfaces* 2018, *10* (46), 39745–39756. https://doi.org/10.1021/acsami.8b14494.
- (46) Długołęcki, P.; Ogonowski, P.; Metz, S. J.; Saakes, M.; Nijmeijer, K.; Wessling, M. On
 the Resistances of Membrane, Diffusion Boundary Layer and Double Layer in Ion Exchange
 Membrane Transport. *Journal of Membrane Science* 2010, 349 (1–2), 369–379.
 https://doi.org/10.1016/j.memsci.2009.11.069.
- 743 (47) Długołęcki, P.; Anet, B.; Metz, S. J.; Nijmeijer, K.; Wessling, M. Transport Limitations 744 in Ion Exchange Membranes at Low Salt Concentrations. *Journal of Membrane Science* 745 **2010**, 346 (1), 163–171. https://doi.org/10.1016/j.memsci.2009.09.033.
- (48) Huang, Y.; Fan, H.; Yip, N. Y. Influence of Electrolyte on Concentration-Induced
 Conductivity-Permselectivity Tradeoff of Ion-Exchange Membranes. *Journal of Membrane Science* 2023, 668, 121184. https://doi.org/10.1016/j.memsci.2022.121184.
- 749 (49) Zhu, S.; Kingsbury, R. S.; Call, D. F.; Coronell, O. Impact of Solution Composition on 750 the Resistance of Ion Exchange Membranes. *Journal of Membrane Science* **2018**, *554*, 39– 751 47. https://doi.org/10.1016/j.memsci.2018.02.050.
- (50) Sarapulova, V. V.; Titorova, V. D.; Nikonenko, V. V.; Pismenskaya, N. D. Transport
 Characteristics of Homogeneous and Heterogeneous Ion-Exchange Membranes in Sodium
 Chloride, Calcium Chloride, and Sodium Sulfate Solutions. *Membr. Membr. Technol.* 2019,
 1 (3), 168–182. https://doi.org/10.1134/S2517751619030041.
- 756 (51) Manning, G. S. Nonconvective Ionic Flow in Fixed-Charge Systems. *J. Chem. Phys.* **1967**, *46* (6), 2324–2333. https://doi.org/10.1063/1.1841040.
- 758 (52) Kenney, J. F.; Keeping, E. S. *Mathematics of Statistics*, 3rd ed.; Van Nostrand: New York, 1954.
- 760 (53) Tedesco, M.; Hamelers, H. V. M.; Biesheuvel, P. M. Nernst-Planck Transport Theory for
 761 (Reverse) Electrodialysis: II. Effect of Water Transport through Ion-Exchange Membranes.
 762 Journal of Membrane Science 2017, 531, 172–182.
- 763 https://doi.org/10.1016/j.memsci.2017.02.031.

- 764 (54) Ji, Y.; Luo, H.; Geise, G. M. Specific Co-Ion Sorption and Diffusion Properties Influence
 765 Membrane Permselectivity. *Journal of Membrane Science* 2018, 563, 492–504.
 766 https://doi.org/10.1016/j.memsci.2018.06.010.
- 767 (55) Cassady, H. J.; Cimino, E. C.; Kumar, M.; Hickner, M. A. Specific Ion Effects on the 768 Permselectivity of Sulfonated Poly(Ether Sulfone) Cation Exchange Membranes. *Journal of* 769 *Membrane Science* **2016**, *508*, 146–152. https://doi.org/10.1016/j.memsci.2016.02.048.
- 770 (56) Li, W.-W.; Yu, H.-Q.; Rittmann, B. E. Chemistry: Reuse Water Pollutants. *Nature* **2015**, 771 528 (7580), 29–31.
- 772 (57) McCartney, S. N.; Watanabe, N. S.; Yip, N. Y. Emerging Investigator Series:
 773 Thermodynamic and Energy Analysis of Nitrogen and Phosphorous Recovery from
 774 Wastewaters. Environmental Science: Water Research & Technology 2021, 7 (11), 2075–
 775 2088.
- 776 (58) Flexer, V.; Baspineiro, C. F.; Galli, C. I. Lithium Recovery from Brines: A Vital Raw Material for Green Energies with a Potential Environmental Impact in Its Mining and Processing. *Sci. Total Environ.* **2018**, *639*, 1188–1204. https://doi.org/10.1016/j.scitotenv.2018.05.223.
- 780 (59) Sata, T. Studies on Anion Exchange Membranes Having Permselectivity for Specific Anions in Electrodialysis Effect of Hydrophilicity of Anion Exchange Membranes on Permselectivity of Anions. *Journal of Membrane Science* **2000**, *167* (1), 1–31. https://doi.org/10.1016/S0376-7388(99)00277-X.
- 784 (60) Sata, T.; Sata, T.; Yang, W. Studies on Cation-Exchange Membranes Having 785 Permselectivity between Cations in Electrodialysis. *Journal of Membrane Science* **2002**, *206* 786 (1–2), 31–60. https://doi.org/10.1016/S0376-7388(01)00491-4.
- 787 (61) Wang, R.; Duddu, R.; Lin, S. Extended Donnan-Manning Theory for Selective Ion 788 Partition and Transport in Ion Exchange Membrane. *Journal of Membrane Science* **2023**, 789 681, 121782. https://doi.org/10.1016/j.memsci.2023.121782.